# Multi-Faceted Free Space Image Distributor for Optical Interconnects in Massively Parallel Processing

F. Zhao[1], E. E. E. Frietman*, Z. Han, R. T. Chen

Microelectronics Research Center, University of Texas at Austin, 10100 Burnet Road, Austin, TX 78710-1100

*Computational Group, Dept. of Applied Physics, Delft University of Technology

Lorentzweg 1, 2628 CJ, Delft, the Netherlands

## ABSTRACT

A characteristic feature of a conventional von Neumann computer is that computing power is delivered by a single processing unit. Although increasing the clock frequency improves the performance of the computer, the switching speed of the semiconductor devices and the finite speed at which electrical signals propagate along the bus set the boundaries. Architectures containing large numbers of nodes can solve this performance dilemma, with the comment that main obstacles in designing such systems are caused by difficulties to come up with solutions that guarantee efficient communications among the nodes. Exchanging data becomes really a bottleneck should all nodes be connected by a shared resource. Only optics, due to its inherent parallelism, could solve that bottleneck. Here, we explore a multi-faceted free space image distributor to be used in optical interconnects in massively parallel processing. In this paper, physical and optical models of the image distributor are focused on from diffraction theory of light wave to optical simulations. The general features and the performance of the image distributor are also described. The new structure of an image distributor and the simulations for it are discussed. From the digital simulation and experiment, it is found that the multi-faceted free space image distributing technique is quite suitable for free space optical interconnection in massively parallel processing and new structure of the multifaceted free space image distributor would perform better.

**Keywords:** free space image distributor, optical interconnection, massively parallel processing

## 1. INTRODUCTION

There is a broad consensus that major discoveries in key sciences would be within reach if computers were far more powerful than today's conventional supercomputers. (See the 1993 published survey of the Committee on Physical, Mathematical and Engineering Sciences in Grand Challenges: High Performance Computing and Communications Report.) Only massively parallel processors are eligible to provide teraflops of computing power in solving problems containing trillions of data points and accessing terabytes of data. Such teraflop performance, derived from the product of the number of nodes and the processing power of each node, can be achieved not only through the use of large numbers of nodes but also from fundamental improvements in hardware technologies and the communication among algorithms. It should be realized that large concentrations of nodes, linked by conventional busses, suffer from communication congestion. This phenomenon, known as the von Neumann bottleneck, is caused by bus contention as busses line up the processed data when exchanging information between the nodes. Optics, due to its inherent parallelism, could solve that bottleneck. Notwithstanding its indisputable success in telecommunications, optical interconnects in massively parallel processors at a crate-to-crate, node-to-node, chip-to-chip or gate-to-gate level are still only sporadically applied. Our research specializes in optically and physically modelling an opto electronic processing & networking system. The goal of the research is to develop optical bus technologies that can be implemented in the next generation of massively parallel processors. We have proposed an multi-faceted free space image distributor system for optical interconnects in massively parallel processing[1]. In this paper, physically and optically modelling multi-faceted free space image distributor for optical interconnects in massively parallel processing is presented. First of all, the general features of the image distributor are described. Then, we focus on the physical and optical models of the image distributor from the diffraction theory of light wave. After that, simulation results are given based on the physically and optically modelling.

[1] Home country address: Dept. of Applied Physics, Harbin Institute of technology, Harbin, 150001, China

Part of the SPIE Conference on Optoelectronic Interconnects VI
San Jose, California • January 1999
SPIE Vol. 3632 • 0277-786X/99/$10.00

Later, new structure of the image distributor is discussed and the simulation results for it are given. Finally, the conclusions complete the paper.

## 2. GENERAL FEATURES OF THE MULTI-FACETED FFREE SPACE IMAGE DISTRIBUTOR

### 2.1 Connecting a node to a free space image distributor

Input/Output in multiprocessor systems, heading for low latency and high bandwidth, is mainly oriented towards solutions that compensate for arrears in improvements in CPU and main memory speeds. In most case, people often concern solutions where each node performs its I/O activities through a low latency organized output port and a parallel accessible input port. The final goal is to adapt the node's structure (illustrated but not described in detail) to simultaneously process the information of all the nodes, with a special emphasis on the input device, because it is the only place where optics inherent parallelism can be maintained up to the level of electronics within the node. We have proposed a scheme for optical interconnects in massively parallel processing[2,3]. Figure 1 shows a block diagram of the scheme, (a), a picture of the parallel accessible photonic integrated circuit (PIC), known as the POWERRAM (b) and an illustration of a multifiber connector linking the PIC to the free space oriented image distributor(c).

In this design, each node contains one or more processors (only one vector processor is shown), a program memory that stores the programs to be executed, a routing or communication processor unit (RPU) that directs data and program streams from and to the optical image distributor and an output buffer that delivers the optically transformed results through a 64-channel wide multi-mode fiber ribbon to the free space oriented image distributor. A second set of multi-mode fiber ribbons leads the 256×256 rays of information from the image distributor to the surface of the PIC.

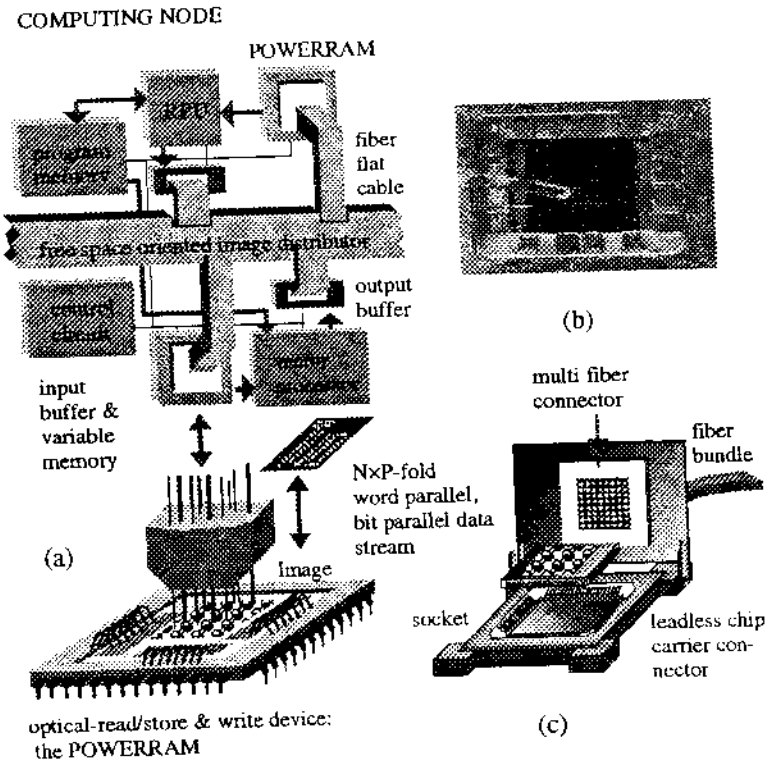


Figure 1. Block diagram of an imaginary node (a), picture of the POWERRAM (b)illustration of a multifiber based POWERRAM connector(c).

### 2.2 Prototyping a 9-faceted free space image distributor

A prototype of a 9-faceted free space image distributor (Here called as the Kaleidoscope), linking nine nodes each of them producing sixty-four bits of data (corresponding with a 26×26 spot array), has been developed[4].

Multiple imaging of large data arrays is obtained by dividing collimated beams from an object into separate bundles by means of refocussing the information with separate lenses or with a multi-facet mirror or prism. Imaging optics and

dividing elements can also be integrated in applying transparent of reflective optics. Several alternatives are possible in designing a free space image distributor, emphasizing compactness and cost effectivity.

In prototyping the Kaleidoscope, the decision was made to focus on a combination of a single lens and a plane facet mirror. See figure 2(a) for a schematic diagram. Increasing the fan-out by cascading multiple (identical manufactured) Kaleidoscopes is accomplished by integrating beamsplitters in the first collimated beam. Rays traced from the object plane at left (see figure 2(b)), propagating through the system to the facet mirror (one facet is shown) at right are reflected back through the same lens system to two-axis image planes. The object image was ± 1 cm above the main axis. The photograph of the Kaleidoscopic prototype is shown in figure 3 (a).

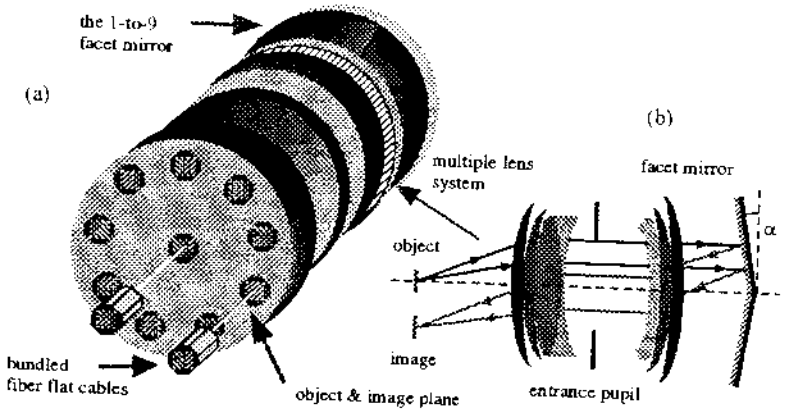


Figure 2 Schematic diagram of the 9-faceted Kaleidoscope (a), and its lens system (b).

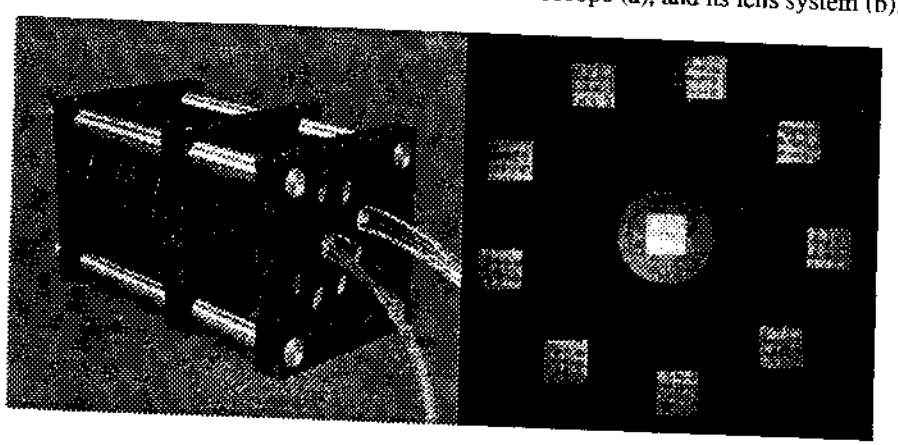

(a) (b)

Figure 3 Photograph of the Kaleidoscopic prototype (a) and its performance (b), (Photograph of the intensity distribution of a 13×13 pixel array)

In order to prove the feasibility of the free space image distributing technique of the Kaleidoscope, experiments were performed. Laser light 2-dimensional arrays of pixels, measuring 7×7, 13×13, 26×26 and 50×50, have been generated and then projected onto the glass area in the middle. The separate spots, occupying an area of 1 $cm^2$, were ~ 300 μm in diameter.

Figure 3(b) shows a 13×13 spot array directly photographed from the image plane, corresponding with the front of the Kaleidoscope. This 13×13 spot array was produced as objects, using two-dimensional Dammann grating, with a diffraction efficiency of 64% and a uniformity of less than 1%. The object area of the central input as well as the surrounding nine distributed images at the outside is displayed. The 50×50 pixel array could not be clearly distinguished by the eye because of the coarse scattering regions on the circular glass screen. The degree of parallelism (the maximum

number of spots in the array) that can be achieved with this Kaleidoscopic prototype is limited by the image quality through optical aberrations in the lens system. An increase of the number of facets on the mirror to broadcast to more than nine outputs restricts the optical aperture and lowers the imaging resolution.

## 3. PHYSICALLY MODELLING A FREE SPACE IMAGE DISTRIBUTOR

An operational formalism, first introduced by Nazarathy et al[5], is applied in modelling the free space oriented image distributing system. The starting point in defining that formalism is the expression of the paraxial approximation of the conventional Fresnel-Kirchhoff integral:[6]

$$u_2(\rho_2) = \frac{\exp\{jkz_{21}\}}{j\lambda z_{21}} \int \exp\left\{\frac{jk(\rho_2 - \rho_1)^2}{2z_{21}}\right\} u_1(\rho_1) d\rho_1 \qquad (1)$$

where $u_2(\rho_2)$, the amplitude distribution on plane $z = z_2$ generated in free space by a field distribution $u_1(\rho_1)$ on plane $z = z_1$; $\lambda$, the wavelength involved; $k = 2\pi/\lambda$; $z_{21} = z_2 - z_1$ the relative spacing between planes $z_2$ and $z_1$ and $\rho = x.\hat{x} + y.\hat{y}$ the transversal radius vector.

Equation 1 can also be rewritten as:

$$u_2(\rho_2) = \left(\frac{\exp\{jkz_{21}\}}{j\lambda z_{21}}\right) \exp\left\{\frac{jk\rho_2^2}{2z_{21}}\right\} \int \left\{u_1(\rho_1) \exp\frac{jk\rho_1^2}{2z_{21}}\right\} \exp\left\{-j2\pi \frac{\rho_2}{2\lambda z_{21}} \rho_1\right\} d\rho_1 \qquad (2)$$

Where

$$\mathcal{F}\left\{u_1(\rho_1) \exp\left\{\frac{jk\rho_1^2}{2z_{21}}\right\}\right\} \equiv \int u_1(\rho_1) \exp\left\{\frac{jk\rho_1^2}{2z_{21}}\right\} \exp\{-j2\pi v\rho_1\} d\rho_1 \Big|_{v = \frac{\rho_2}{2\lambda z_{21}}} \qquad (3)$$

is the two dimensional Fourier transformation of the function described between the brackets {}. With the help of a scaling operator $\mathcal{V}$, a Fourier transform operator $\mathcal{F}$ and a quadratic multiplication operator $Q$, the overall transformation from plane $z_1$ to plane $z_2$ can be expressed as a single operator -- the Fresnel free-space propagation operator {FPO}, resulting in:

$$\mathcal{R}[z_{21}] = \frac{e^{jkz_{21}}}{j\lambda z_{21}} Q\left[\frac{1}{z_{21}}\right] \mathcal{V}\left[\frac{1}{\lambda z_{21}}\right] \mathcal{F} Q\left[\frac{1}{z_{21}}\right] \qquad (4)$$

and consequently $u_2(\rho_2) = \mathcal{R}[z_{21}]u_1(\rho_1)$.

### 3.1 Applying the operator approach to a free space image distributor

Properties of rays travelling through an optical system can be formulated according to a matrix formalism, which in many aspects is the geometrical-optics equivalent of the operator methods described by VanderLugt , Butterweck and Nazarathy and Shamir. In applying these methods, only meridional rays have to be considered, that propagate in plane surfaces that contain the z-axis. In case an optical system imposes circle-symmetrical properties the transverse axis $y_r$, revolving on the z-axis, arranges a cylinder in which any arbitrary plane $\{y_r, z\}$ can be denied. In conclusion: there is always a $\{y_r, z\}$ plane surface available in considering an M×M matrix of mutually independent propagating rays. The matrix, reflected in this paper, is of size 256×256.

The way the information propagates through an optical system, containing lenses, mirrors and free space sections, can be described by an overall transfer operator $\mathcal{T}$. This operator, expressing a relationship between an input field $U_i$ and its response at the output $U_o$, answers the following relation:

$$U_o = \mathcal{T} U_i \qquad (5)$$

Where $\mathcal{T}$originates from a product of the basic operators $\mathcal{V}$, $\mathcal{F}$, $Q$and $\mathcal{R}$.[5]

The system to be modelled , which is shown in Fig.4, consists of two spherical lenses with focal lengths $f_1$ and $f_2$ respectively and a slightly tilted mirror, revolving on the x-axis according to an angle $\alpha$.

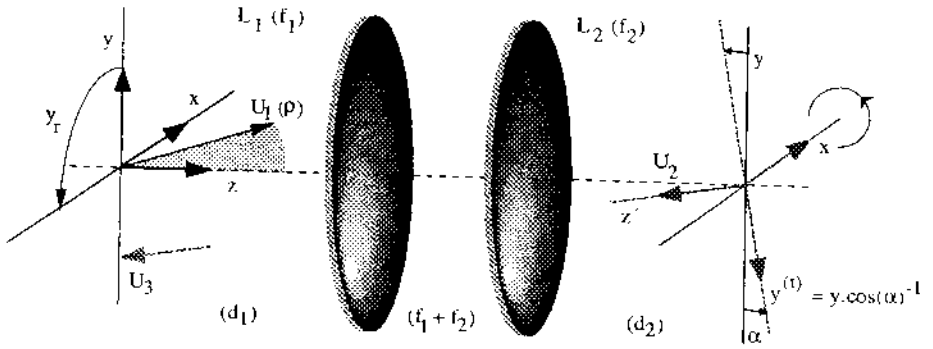


Figure 4. The foundations of the free space image distributor.

First the complex field $U_2\{x,y^{(t)}\}$ is depicted across a plane $\{x,y^{(t)}\}$ (represented by the surface of the tilted mirror) located to the right of lens $L_2(f_2)$ as a result of the information $U_1\{x,y\}$ propagating through the system and reflecting against the tilted mirror. The relation is described as:

$$U_2\left\{x,y^{(t)}\right\} = U_1\left\{x,y\right\}\mathcal{V}\left[1,-\frac{1}{\cos(\alpha)}\right]e^{-j\frac{4\pi y\tan(\alpha)}{\lambda}} \Rightarrow U_2\left\{x,y^{(t)}\right\} = U_1\left\{x,-\frac{y}{\cos(\alpha)}\right\}e^{-j\frac{4\pi y\tan(\alpha)}{\lambda}} \tag{6}$$

Where $U_1(x,y,\alpha)$, after being reflected against the tilted mirror, represents the result when implementing the scaling process

$$\mathcal{V}\left[1,-\frac{1}{\cos(\alpha)}\right]e^{-j\frac{4\pi y\tan(\alpha)}{\lambda}} \tag{7}$$

at the tilted axis $y^{(t)}$. $U_2\{x,y^{(t)}\}$ for small $\alpha$'s yields:

$$U_2\left\{x,y^{(t)}\right\} \cong U_1\left\{x,-y\right\}e^{-j\frac{4\pi\alpha y}{\lambda}} \quad \textit{for small } \alpha \tag{8}$$

After being reflected by the tilted mirror, the rays travel back through the same lens system and arrive at the original plane $\{x,y\}$ at the left of lens $L_1(f_1)$. The complex field $U_3\{x,y\}$, resulting from $U_2\{x,y^{(t)}\}$, again springs from a product containing a multiplication factor $Q$, a scaling factor $\mathcal{V}$and a Fourier operator $\mathcal{F}$, respectively.

$$U_3\left\{x,y\right\} = \mathcal{T}_{bw}\,U_2\left\{x,y^{(t)}\right\} \Rightarrow \mathcal{T}_{bw}\,U_1\left\{x,-y\right\}e^{-j\frac{4\pi\alpha y}{\lambda}} \quad \textit{for small } \alpha \tag{9}$$

Where $\mathcal{T}_{bw}$ indicates the backwards overall transfer operator. The situation is considered with the object located on the focal plane.

### 3.2 On focal plane approach

Optical information, travelling from the object (front) plane to the tilted mirror (backplane) through two positive lenses $L_1$ and $L_2$, with focal length of $f_1$ and $f_2$ respectively, undergoes a sequence of two Fourier Transforms yielding the following relation:

$$\mathcal{R}\left[z_{21}\right] = e^{jkz_{21}}\mathcal{V}\left[\frac{1}{\lambda f_2}\right]\mathcal{F}\,\mathcal{V}\left[\frac{1}{\lambda f_1}\right]\mathcal{F} \tag{10}$$

In the on-focal plane situation, $d_1$ ($\equiv f_1$) and $d_2$ ($\equiv f_2$) represent the distance from the front lens $L_1(f_1)$ to the object plane and from the back lens $L_2(f_2)$ to the tilted mirror respectively, see figure 2. In acquiring an expression for the transfer operator, the survey of the various operators as described in section 5.4.1 of Goodman is used: [6]

$$\begin{aligned}
&\mathcal{F}\,\mathcal{V}\left[\frac{1}{\lambda f_1}\right] = \mathcal{V}\left[\lambda f_1\right]\mathcal{F}\\
&\mathcal{F}\,\mathcal{F} = \mathcal{V}\left[-1\right]\\
&\mathcal{V}\left[\frac{1}{\lambda f_2}\right]\mathcal{V}\left[\lambda f_1\right] = \mathcal{V}\left[\frac{f_1}{f_2}\right]
\end{aligned} \tag{11}$$

Introducing (11) into equation (10) results in:

$$\mathcal{V}\left[\frac{1}{\lambda f_2}\right]\mathcal{F}\,\mathcal{V}\left[\frac{1}{\lambda f_1}\right]\mathcal{F} \Rightarrow \mathcal{V}\left[\frac{1}{\lambda f_2}\right]\mathcal{V}[\lambda f_1]\,\mathcal{F}\,\mathcal{F} = \mathcal{V}\left[\frac{f_1}{f_2}\right]\mathcal{V}[-1] = \mathcal{V}\left[-\frac{f_1}{f_2}\right] \tag{12}$$

$$U_2\{x,y\} = e^{jkz_{21}}\mathcal{T}\,U_1\{x,y\} \Rightarrow e^{jkz_{21}}\mathcal{V}\left[-\frac{f_1}{f_2}\right]U_1\{x,y\}$$

The resulting complex field $U_2\{x, y\}$ demonstrates that information $U_1\{x, y\}$ arrives both inverted and scaled by a factor $[-f_1/f_2]$ at the tilted mirror.

Going backwards in the modelling process, this way considering the complex field $U_2\{x,y^{(t)}\}$ as the input of the optical system and $U_3\{x, y\}$ as the corresponding output, yields a transfer operator $\mathcal{T}_{bw}$. From equations 8 and 12, the result for $U_3\{x, y\}$ is defined as:

$$U_2\{x,y^{(t)}\} = e^{jkz_{21}}\mathcal{V}\left[-\frac{f_1}{f_2}\right]U_1\{x,y\}\,\mathcal{V}[1,-1]\,e^{-j\frac{4\pi\alpha y}{\lambda}}$$

$$\mathcal{R}[z_{12}] = e^{jkz_{12}}\,\mathcal{V}\left[\frac{1}{\lambda f_1}\right]\mathcal{F}\,\mathcal{V}\left[\frac{1}{\lambda f_2}\right]\mathcal{F} \Rightarrow$$

$$\Rightarrow e^{jkz_{12}}\mathcal{V}\left[\frac{1}{\lambda f_1}\right]\mathcal{V}[\lambda f_2]\,\mathcal{F}\,\mathcal{F} = e^{jkz_{12}}\mathcal{V}\left[\frac{f_2}{f_1}\right]\mathcal{V}[-1] = e^{jkz_{12}}\mathcal{V}\left[-\frac{f_2}{f_1}\right]$$

$$U_3\{x,y\} = \mathcal{R}[z_{12}]U_2\{x,y^{(t)}\} = e^{jkz_{12}}\mathcal{V}\left[-\frac{f_2}{f_1}\right]U_2\{x,y^{(t)}\}$$

$$\Rightarrow e^{jkz_{12}}\mathcal{V}\left[-\frac{f_2}{f_1}\right]e^{jkz_{21}}\mathcal{V}\left[-\frac{f_1}{f_2}\right]U_1\{x,y\}\,\mathcal{V}[1,-1]\,e^{-j\frac{4\pi\alpha y}{\lambda}} \tag{13}$$

$$= e^{jkz_{12}}e^{jkz_{21}}\mathcal{V}[1]\,U_1\{x,y\}\mathcal{V}[1,-1]\,e^{-j\frac{4\pi\alpha y}{\lambda}}$$

$$= e^{jk(z_{21}+z_{21})}\,U_1\{x,y\}\mathcal{V}[1,-1]\,e^{-j\frac{4\pi\alpha y}{\lambda}}\Big|_{for\ small\ \alpha's}$$

In conclusion; when propagating forward and backwards through the free space imaging distributor, the result $U_3\{x, y\}$ at the front surface, which in the on-focal plane situation behave as object as well as image plane, equals the original information $U_1\{x, y\}$ scaled by a constant V [1, -1].

## 4. SIMULATIONS FOR THE 9-FACETED FREE SPACE IMAGE DISTRIBUTOR

Simulations with the CODE V program evaluate the resolving capabilities of an optical system, that duplicates a single 26×26 sized input (the object) to in this case nine 26×26 sized replicas (the images). CODE V is a registered trademark of Optical Research Associates at Pasadena, California.

### 4.1 Simulations of the Modulation Transfer Function

Determining an optical system's MTF is identical to appointing the spatial frequency response $\omega_r$.. Simulations are performed as a function of different wavelengths of which the individual components are mutually weighed. The MTF is calculated from either wavefront data (OPD), resulting in the diffraction MTF, or from transverse ray aberration data, yielding the geometrical MTF. Generally, the use of a geometrical MTF is restricted to situations where the RMS spot size is significantly larger than the diffraction limited spot size. See the CODE V manual for the details. [7]

Figure 5(b), of which the abscissa scale is normalized to unity at cut-off frequency $\omega_{co}$, illustrates three different cases. Curve (a) represents the MTF of an aberration free lens with a circular aperture, the resolving limit occurring when the spatial frequency is equal to $2NA/\lambda$. Curve (b) indicates a situation with a 25% central obstruction, and curve (c) demonstrates the effects of a 50% obstruction.

It must be realized that curve (a) is not a complete straight line. The result is always positive and strictly bandlimited to a cut-off frequency $\omega_{co}$. [8]

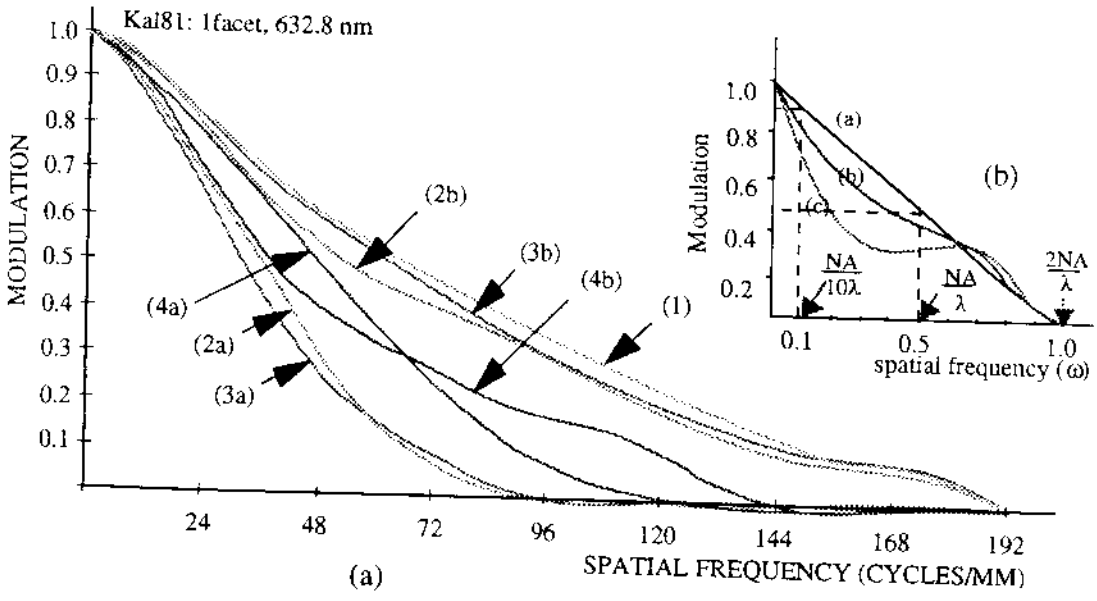


Figure 5. Results of the simulations of the MTF for three field angles (a) and an illustration of three particular cases (b).

Computed at a single wavelength λ of 632.8 nm, figure 5(a) shows the results of the diffraction limit (1) and the tangential and radial MTFs for each field angle position at a 0.0 field {(2a) resp. (2b): 0.01°}, a +1.0 field {(3a) resp. (3b): 0.00°} and a -1.0 field {(4a) resp. (4b): 0.52°}. The horizontal axis ranges from 0 to 192 cycles/mm. The vertical axis, representing the modulation depth, varies from 0 to 1.0. Central obscurrations, mostly indicated by crossover points in the resulting graph, generally enhance the high frequency MTF at the cost of a reduction of the mid-frequency components.

Figure 5 also indicates that a spatial frequency of roughly 12 cycles/mm is achieved giving concrete form to results at a 0.9 MTF modulation depth.

### 4.2 Simulations of the Point Spread Function

The image quality of professional available optical systems is so well corrected for aberrations that it can be termed diffractionally limited. Yet it would be useful to know their theoretical limitations. A PSF analysis, characterizing the performance of an image for a point object in its image plane, is able to illustrate that. In the presence of aberrations, generally a spot diagram is used, that originates from a geometrical tracing of a number of rays.

Using CODE V, PSF computes the wave aberration of a system and by executing a Fast Fourier Transformation (FFT) determines the diffraction image shape in the designated focal plane integrated over the wavelengths according to the weights assigned. The resulting image patch is achieved by calculating a grid across the image itself with the chief ray or optical axis as the center point of the grid.

The PSF intensity distribution is plotted as a three-dimensional solid. The result, considering an axial symmetric system, is a series of accumulating rings with decreasing diameter around a central bright core. It is obvious that the central core contains only a fraction of the total energy distribution of the PSF. Such results, simulated at different field angles and printed in perspective with the light intensity defined along the vertical axis, are plotted in figure 6. See Goodman [6] for a theoretical analysis.

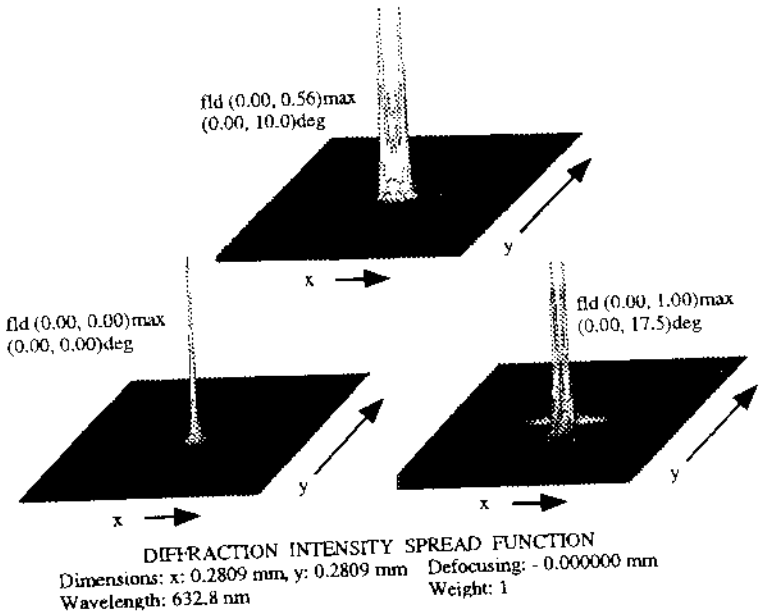


Figure 6. Various Diffraction Intensity Spread Functions.

### 4.3 Point spread function simulations at three different wavelengths

In defining properties of laser-based or other quasi-monochromatic systems, CODE V requires at least one wavelength to perform first order calculations and to trace the reference rays. For the polychromatic category, two more wavelengths are required to explore systems that use different light sources and detectors. The second and the third wavelength, are mostly used for paraxial calculations and for tracing their reference rays. Each wavelength carries its own weight, according to a simple 1-2-1 weighting scheme. Figure 7 shows the diffraction intensity spread function for the 643.8, 546.1 and 480.0 nm wavelengths respectively.

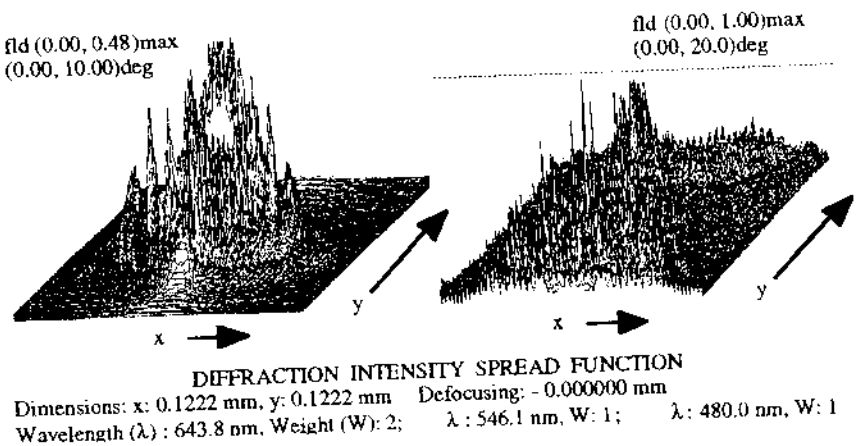


Figure 7. Three wavelengths organized Diffraction Intensity Spread Functions.

### 4.4 Spot diagrams

Spot diagrams, demonstrating a geometrical structure of an image in a non-diffraction-limited system, are generated by propagating an evenly spaced grid of rays from each object point on the entrance pupil. The number of rays that are traced is proportional to the system wavelength weights. A hundred rays are generally sufficient to give an impression of the performance. Figure 8 displays three horizontally field positions as a function of multiple vertically organized 50 μm scaled focal positions. The spot size at a field angle of 10.00 and 17.50 degrees is respectively 50 and 150 μm.

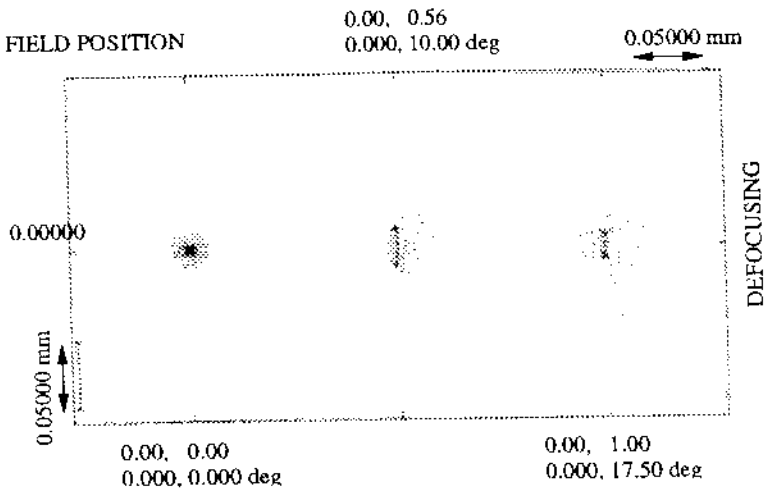


Figure 8 Spot diagram of the Kaleidoscopic system

## 5. A LARGE-SCALE (N>9) SUCCESSOR

As an extension of the research focused on designing the 9-faceted Kaleidoscope, different multiple imaging techniques were investigated to linking a larger number (N>9) of computing nodes. In considering MPPs with 1024 (or more) fully connected nodes, each of them producing 64 bits of information, the only alternative left is to explore free space imaging techniques. It is without any doubt that a *relatively slow* (0.5 Gb/s/link) but cheap parallel data distributing system is preferred over an ultra fast (10 Gb/s) but expensive serial solution as used by telecommunications.

Going back and forth through the same objective make aberration and distortion worse. A single lens with less distortion and a high resolution will improve on that. In any one wavelength, for an object at a fixed distance and the aperture diaphragm at a given position, the properties of an optical system are defined by the five Seidel aberrations, called the spherical aberration, the coma, the astigmatism, the Petzval curvature and the distortion. Without going into details it has been proven that the coma is the most objectionable of all aberrations since it depends on the bending of the lens. According to the widely adopted suggestion of Abbe, optical systems without spherical aberration and coma are referred to as aplanatic systems. In exploiting solutions to minimize the influence of the coma, a lens can be designed for which the center of the curvature of each surface coincides with that of the mirror. The features of such a concentric lens system are demonstrated by the property that since each surface is centered at the position of the object, also each principal ray is incident normally at all surfaces in case the stop is also at the position of the object. If the lens is properly ground and manufactured no coma and astigmatism should occur. See figure 9 for an illustration of a 16-faceted concentric lens based Kaleidoscope. The facet mirror is moved to the front and a spherical mirror has taken its place. The lens and the mirror are concentrically arranged.

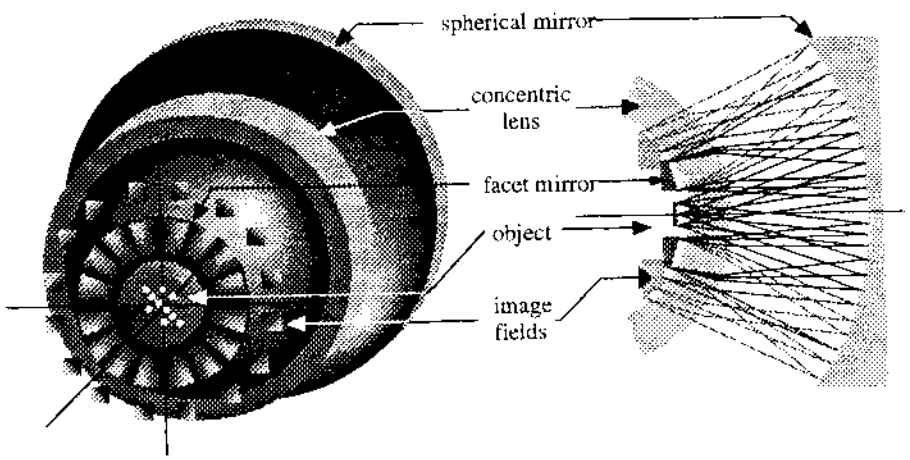


Figure 9 Schematic diagram of a 16-faceted concentric lens based Kaleidoscope.

In this phase of the design only simulations, performed with CODE V, have been executed to indicate the intrinsic properties of the system. It suffices to accentuate the important issues.

### 5.1 The modulation transfer function

Simulating an optical system is in effect an exploration at low cost, that is to say no actual manufacturing is required. To be more precisely, point spread and modulation transfer functions on the one hand and spot diagrams on the other give a clear insight of the properties of a complex lens system, but physical experiments are always necessary to prove the feasibility of the idea.

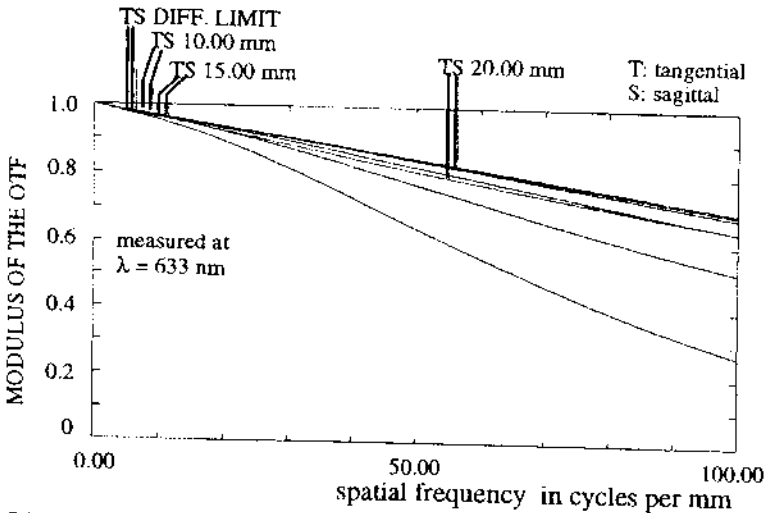


Figure 10 The results of the modulation transfer function for various field angles.

Figure 10 shows the tangential (T) and sagital (S) responses at diffraction limit (TS DIFF.LIMIT) and at 10, 15 and 20 mm field angle position respectively. All were computed at $\lambda$ = 633 nm. The horizontal axis, representing the spatial frequency, ranges from 0 to 100 cycles/mm. The vertical axis, representing the modulus of the OTF, varies from 0 to 1.0. The spatial frequency at a 90% modulation depth for the different situations varies slightly around the 25 cycles per mm.

### 5.2 The point spread function

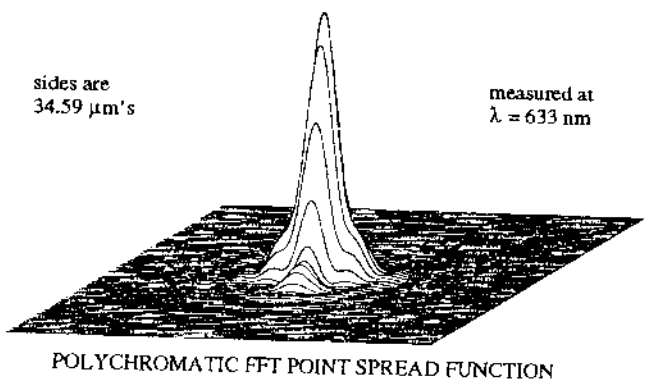


Figure 11 The results of a single diffraction intensity spread function.

The image quality of the *concentric lens* configuration, computed at a single wavelength $\lambda$ = 633 nm, is deduced from processing the PSF. Simulations were performed at a field angle of 10 mm. The x and y sides, both 34.59 µm wide.

demonstrate the features of this design. The results are shown in figure 11. The intensity distribution is plotted as a three-dimensional solid. The diameter of the pedestal, the lowest of the series of accumulating rings, is roughly 10 µm. No noticeable differences were found when different field angles were simulated.

### 5.3 Spot diagrams

Spot diagrams are mostly derived from propagating an evenly spaced grid of rays. A hundred rays are generally sufficient to give an impression of the performance.

Figure 12 displays a through focus spot diagram defined at three different field angles (10, 15 and 20 mm) as a function of five different focusing situations (-20, -10, 0, +10 , +20). The resolution of the horizontal and vertical positions is appointed 10 µm. All spots are smaller than the indicated 10 µm. Compare the results of the figure's 10, 11 and 12 with those of the figure's 5, 6 and 8. The size of the spots has decreased, the number of cycles/mm of the spatial frequency has increased and the design of a 1-to-16 or 1-to-32 faceted Kaleidoscope only requires a single concentric lens.

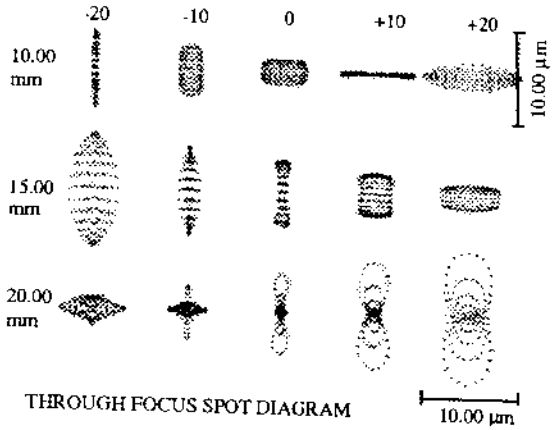


Figure 12 The results of the spot diagram.

## 6. CONCLUSIONS

Electronic backplanes will probably fail to meet the necessary interconnect densities for large scale computers, but optical techniques appear to hold promise. So studying interconnect requirements for node-to-node level applications, particularly at massively parallel processors, comes down to efficiently exploring and exploiting optics inherent parallelism. Here, The features of free space image distributing techniques for optical interconnection in massively parallel processing were studied and solutions were proposed that favor the development, prototyping and testing of a free space oriented 9-faceted kaleidoscopic system and designing a large-scale (N>9) successor. Physically and optically modelling and the simulations are emphased on. The results show that the multi-faceted free space image distributing technique is one of good schemes in optical interconnection in massively processing and a single concentric lens kaleidoscopic system could perform better.

## ACNOWLEDGMENTS

The authors wish to acknowledge Hedser van Brug of Delft University of Technology for putting his simulation program PipesSA at our disposal.

## REFERENCES

1. Frietman, W van Nifterick, L Dekker, Th.J.M. Jongeling; "Parallel Optical Interconnects implementation of Optoelectronics in Multi-Processor architectures, *Applied Optics*, Vol. 29, pp. 1161-1177, 1990.

2. E. Frietman. *Opto-Electronic Processing & Networking: A Design Study. Perspectives of Optical Interconnects in Massively Parallel Processing*, Research Monograph: ISBN 90-900 8690-0, 1995.

3. E. Frietman and F. Zhao, "A prototype for optical interconnection in massively parallel processing and its physical and optical models", Proc. Of OC'98, Sponsored by EOS, ICO, IEEE/LEOS, OSA and SPIE, Brugge, Belgium, June 17-20, 1998.

4. E. Frietman and F. Zhao, "Optical multifaceted free space image distributor for massively parallel processing", Proc. Of the Fifth International Conference on Massively Parallel Processing Using Optical Interconnections, Sponsored by IEEE, Las Vegas, Navada, USA, June 15-17, 1998.

5. Nazarathy, J. Shamir; "Fourier optics described by operator algebra". J. Opt. Soc. Am., Vol. 70, pp.150-159, 1980,.

6. Goodman. *Introduction to Fourier Optics, 2nd edition.* McGraw-Hill, New York, 1996.

7. *CODE V Reference Manual, Volume II.* Optical Research Associates, Pasadena, California, USA, 1994.

8. Young. Image Fidelity: *Characterizing the Imaging Transfer Function.* Chapter I of Fluorescence Microscopy of living cells in Culture, part B: Methods in Cell Biology, Academic Press, Inc Harcourt Brave Jovanovich, Publishers, San Diego, USA, Vol. 30, pp.1-45.